

## Report

# ROCK- and Myosin-Dependent Matrix Deformation Enables Protease-Independent Tumor-Cell Invasion In Vivo

Jeffrey B. Wyckoff,<sup>1</sup> Sophie E. Pinner,<sup>2</sup>  
Steve Gschmeissner,<sup>2</sup> John S. Condeelis,<sup>1</sup>  
and Erik Sahai<sup>2,\*</sup>

<sup>1</sup>Analytical Imaging Facility  
Department of Anatomy and Structural Biology  
Albert Einstein College of Medicine  
1300 Morris Park Avenue  
Bronx, New York 10461

<sup>2</sup>Cancer Research UK London Research Institute  
44 Lincoln's Inn Fields  
London, WC2A 3PX  
United Kingdom

## Summary

**Tumor cells invading three-dimensional matrices need to remodel the extracellular matrix (ECM) in their path. Many studies have focused on the role of extracellular proteases [1, 2]; however, cells with amoeboid or rounded morphologies are able to invade even when these enzymes are inhibited [3, 4]. Here, we describe the mechanism by which cells move through a dense ECM without proteolysis. Amoeboid tumor cells generate sufficient actomyosin force to deform collagen fibers and are able to push through the ECM. Force generation is elevated in metastatic MTLn3E cells, and this correlates with increased invasion and altered myosin light chain (MLC) organization. In metastatic cells, MLC is organized perpendicularly to the direction of movement behind the invading edge. Both the organization of MLC and force generation are dependent upon ROCK function. We demonstrate that ROCK regulates the phosphorylation of MLC just behind the invading margin of the cell. Imaging of live tumors shows that MLC is organized in a similar ROCK-dependent fashion in vivo and that inhibition of ROCK but not matrix-metalloproteases reduces cancer cell motility in vivo.**

## Results and Discussion

Breast tumors are surrounded by a collagen-rich matrix [5]; to mimic this environment, we overlaid cultured cells with a collagen I gel [6]. After 24 hr, 20%–25% of MTLn3E cells (A highly invasive subline of MTLn3 cells, MTLn3E overexpresses the epidermal growth factor receptor [7]) had invaded a distance of 20  $\mu\text{m}$  or more (Figures 1A and 1B), whereas fewer than 5% of the nonmetastatic parental MTC cells would invade 20  $\mu\text{m}$ . Invading MTLn3E cells had an amoeboid morphology (Figure 1B); previous work has suggested that cells moving with this morphology do not require extracellular proteases [3, 4]. Figure 1C shows that treatment with GM6001, which blocks a broad range of matrix-metalloproteases (MMPs), did not inhibit the invasion of MTLn3E cells.

Furthermore, blockade of a broad range of serine and cysteine proteases combined with MMP inhibition did not block the invasion of MTLn3E cells (Figure 1C). We confirmed the efficacy of this combination of protease inhibitors by using gelatin zymography (see Figure S1 in the Supplemental Data available with this article online, compare lanes 1 and 2 with 5 and 6). This also revealed that MTLn3E cells only produce small amounts of secreted proteases in comparison to HT1080 cells, which normally use a protease-dependent form of invasion [4] (Figure S1, compare lanes 1, 2, and 4).

To investigate how cells invaded in the absence of proteolysis, we imaged the ECM as cells invaded it. This revealed that collagen fibers were deformed as cells invaded the ECM (Movie S1). We used DQA algorithms [8] to accurately analyze changes in collagen images taken at 1-min intervals; representative images from one such time series together with the output of the DQA algorithms are shown in Figures 1D and 1E. This revealed that the collagen in front of the invading cell was pushed away from the cell. No consistent pattern of deformation was observed at the rear of cells (data not shown). In cases where the cell extended a protrusion that was retracted without leading to translation of the cell body, collagen was pulled toward the cell. By measuring the degree of deformation caused by calibrated microneedles, we estimated that invading MTLn3E cells exerted forces in the range of 10–20 nN. This value is comparable with that measured for fish keratinocytes [9, 10].

Deformation of collagen was observed by both control and GM6001-treated cells, indicating that MMP activity is not required for MTLn3E cells to deform the collagen matrix (Movies S1 and S2). We hypothesized that the force needed to deform the collagen was generated by productive actomyosin interactions [11]. Figure 1E shows that blebbistatin, a nonmuscle myosin ATPase inhibitor [12], dramatically reduced the extent of collagen deformation. Actomyosin activity is regulated by phosphorylation of MLC; therefore, we investigated the effect of inhibiting kinases that can phosphorylate MLC. Inhibition of MLC kinase (MLCK) reduced collagen deformation but also inhibited the formation of cell protrusions (data not shown); from this result, we could not determine if MLCK function is specifically required for force generation or for the initial extension of cell protrusions prior to force generation.

ROCK has also been shown to regulate myosin activity by phosphorylating either the regulatory subunit of MLC phosphatase or MLC directly (because of the high degree of sequence similarity between ROCK1 and 2, we refer to them generically as ROCK) [13, 14]. Inhibition of ROCK by two different structurally unrelated ROCK inhibitors (Y27632 and H1152) significantly reduced collagen deformation (Movie S3 and Figure 1E). Inhibition of ROCK did not affect the low levels of protease activity secreted by MTLn3E cells (Figure S1). Importantly, imaging of the cells revealed that they were still able to extend

\*Correspondence: [erik.sahai@cancer.org.uk](mailto:erik.sahai@cancer.org.uk)

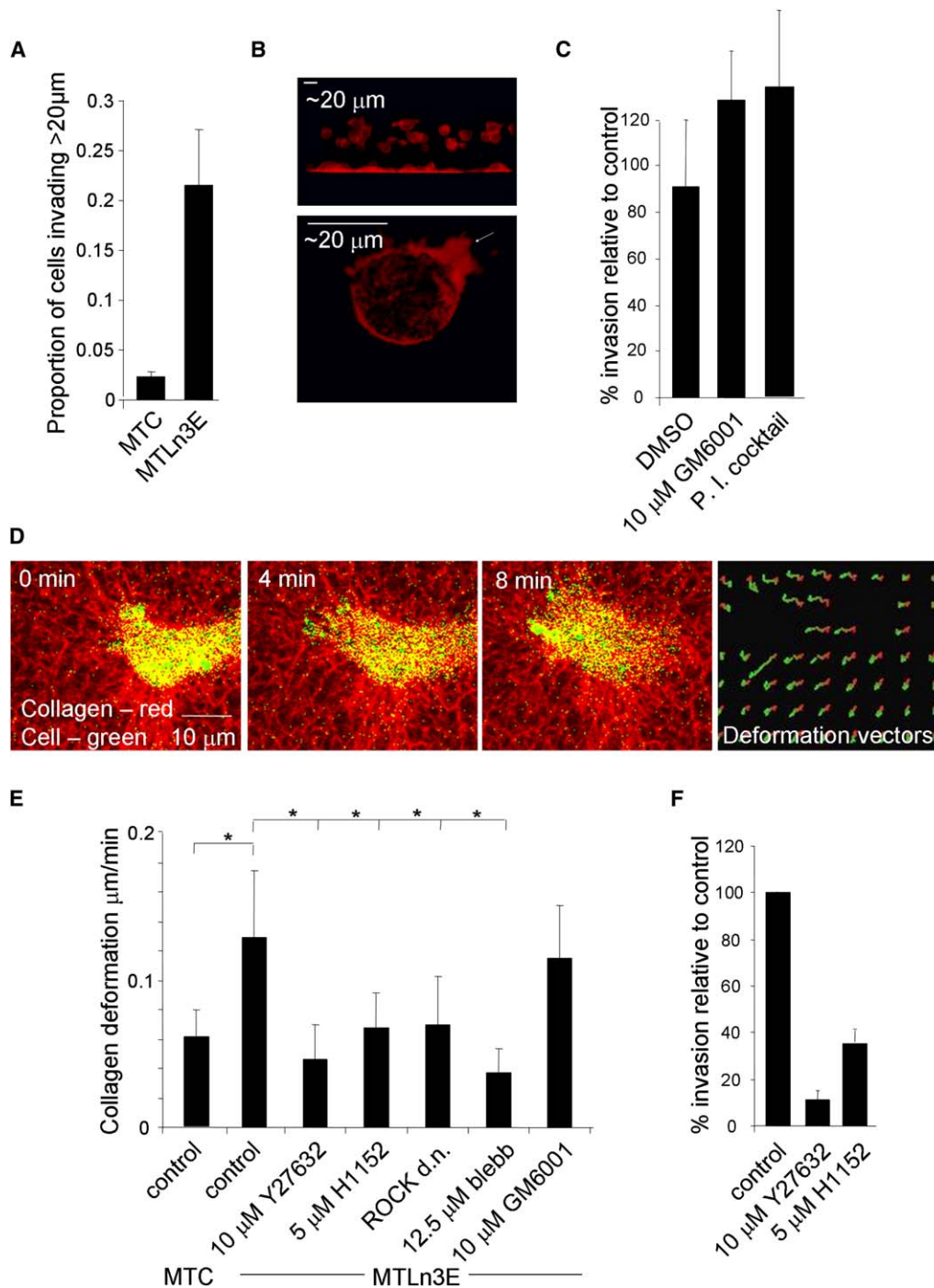


**Figure 1. Collagen Deformation and Invasion Is Protease Independent but ROCK Dependent**

(A) The proportion of MTC and MTLn3E cells invading 20 μm or more in 24 hr is shown. The average of at least three independent experiments with standard errors is shown; typically 200 cells were analyzed for each experimental condition.

(B) Representative three-dimensional reconstructions of MTLn3E cell invasion at either low magnification (upper panel) or high magnification (lower panel) and stained with phalloidin to reveal F-actin; the arrow indicates an invading-actin-rich protrusion.

(C) The effect of 10 μM GM6001 or 10 μM GM6001 + 10 μM Aprotinin + 10 μg/ml Leupeptin on the ability of MTLn3E cells to invade 20 μm or more in 24 hr. The average of at least three independent experiments with standard errors is shown; typically 200 cells were analyzed for each experimental condition.

(D) Three images of an MTLn3E cell (green) invading a collagen I matrix (red) are shown. Bottom-right image shows DQA analysis of collagen I deformation by the cell shown in the other panels. Lines represent vectors of collagen deformation over 8 min; the direction of deformation is running in a red to green direction.

(E) Quantification of the extent of collagen I deformation by MTC or MTLn3E cells from untreated, treated with 10 μM Y27632 and 5 μM H1152, transfected with inhibitory ROCK mutant, treated with 12.5 μM Blebbistatin, or treated with 10 μM GM6001. The average amount of collagen I

protrusions (Figure 2; data not shown); however, these protrusions now extended over the surface of the matrix and did not effectively penetrate into the matrix (compare control cells in Figure 2C<sub>i</sub> to inhibitor-treated cells in Figures 2E<sub>i</sub>–2E<sub>ii</sub>). We performed cell adhesion assays to exclude the possibility that inhibition of ROCK altered the amount of force exerted on the collagen by affecting the cells' ability to adhere to collagen. Figure S2A shows that inhibition of ROCK did not affect the ability of MTLn3E cells to adhere to collagen, although the organization of prominent adhesions at the front of the cell was altered. We speculate that MLCK is required for protrusions to be efficiently formed but is not able to generate sufficient force to deform the collagen matrix; in order for this to occur, ROCK function is required.

If this ROCK-dependent force-mediated mechanism of collagen remodeling is important for invasive and metastatic potential, then invasive cells should generate more force, and reducing force generation should prevent invasion. Comparison of the behavior of metastatic MTLn3E and nonmetastatic MTC cells revealed that MTC cells generate significantly less force (Figure 1E). This difference is not due to altered abilities to bind to collagen I (Figure S2C). Next, we tested to see if the invasion of MTLn3E cells could be prevented by reducing their ability to deform the collagen matrix with ROCK inhibitors; Figure 1F shows that the invasion of MTLn3E cells was significantly reduced by treatment with either Y27632 or H1152. Similar results were obtained by transfection of an inhibitory ROCK construct (data not shown). These results establish that increased ROCK-dependent force generation is required for the invasive behavior of tumor cells.

To gain further insight into the regulation of MLC in the invading MTLn3E cells, we performed time-lapse microscopy by using green fluorescent protein (GFP)-labeled MLC. Figure 2A and Movie S4 show that MLC was organized into bundles that were perpendicular to the direction of movement just behind the F-actin-rich invading edge. MLC was also found around the cortex at the sides and rear of the cell. Reflectance imaging confirmed that the cell was moving within the collagen matrix (data not shown). These data suggest that at the front of the cell, MLC is bundled perpendicularly to the pushing force generated by invading cells. To confirm this, we imaged MLC-mRFP (monomeric Red Fluorescent Protein) in cells invading FITC collagen; Figure 2B shows that the collagen is indeed pushed perpendicularly to the MLC structures at the very front of the cell (area marked "fz"). At the lateral margins (areas marked "lz"), MLC structures are less prominent but are now aligned with the direction of cell movement and force generation; this suggests that some force is applied along the actomyosin network at the sides of the cell.

We performed scanning electron microscopy (SEM) to gain a more detailed insight into the cytoskeleton structure of invading cells. Figure 2C shows the actin cytoskeleton of an invading MTLn3E cell; we confirmed that the filamentous structures observed were F-actin

by treating cells with cytochalasin D to disrupt F-actin. Figure S3 shows that this completely disrupted the mesh in the cell cortex and significantly disrupted the fibers in cell protrusions. Higher-magnification images show F-actin extending in the direction of invasion (marked with asterisks in Figure 2C<sub>iii</sub>); this can also be seen in F-actin staining of control cells in Figure 2A. Further behind these structures is a very dense actin meshwork with frequent bundles that are perpendicular to the direction of invasion (marked with arrowheads in Figures 2C<sub>ii</sub>–2C<sub>iii</sub>); these thick bundles and dense actin mesh are connected to the rest of the actin cortex and are likely to be associated with MLC. Consistent with this, inhibition of nonmuscle myosin ATPase activity with blebbistatin [12] disrupted the dense actin mesh and led to the appearance of flat "fan-like" arrays of F-actin (marked with an arrow in Figure S3B).

In MTC cells, which generate less force than their metastatic counterparts, MLC was recruited to cell protrusions but was not bundled perpendicularly to the direction in which the protrusion was extending (Figure 2D and Movie S5). Similarly, inhibition of ROCK in MTLn3E cells did not prevent MLC from being recruited near the invading edge of the cell but prevented it from being aligned perpendicularly to the direction in which the cell was extending a protrusion (Figure 2D and Movie S7). Transfection of an inhibitory ROCK mutant also disrupted the bundling of MLC (Figure 2D and Movie S8). SEM analysis revealed that inhibition of ROCK function caused cell protrusions to become longer and appear flatter; in particular, the F-actin network just behind the invading edge was much less dense and was oriented in the same direction as the protrusion (Figures 2E<sub>i</sub>–2E<sub>ii</sub>). Because they are extending over the surface of the matrix as opposed to invading into it, the protrusions have a flatter appearance (see also the effect of blebbistatin treatment in Figure S3C). In addition, we observed that the actin meshwork throughout the cell cortex was significantly less dense than in control cells (compare Figures 2C<sub>iv</sub> and 2E), suggesting that ROCK may play a role in regulating contractility of the actin network in the cell cortex. In agreement with this, the localization of MLC to the cell cortex in MTLn3E cells plated on top of collagen I gel is significantly disrupted in cells treated with either 5  $\mu$ M H1152 or 10  $\mu$ M Y27632. However, this is not affected in cells treated with 25  $\mu$ M ML-7 (Figure S4).

To test whether phosphorylation of MLC was required for it to be aligned correctly, we used an MLC mutant with both potential ROCK-regulated phosphorylation sites mutated to alanine [15]; Figure 3A and Movie S9 show that nonphosphorylated MLC can not be bundled in the extending cell protrusion. Expression of this mutant also reduced the invasion of MTLn3E cells (Figure 3B) and modestly reduced collagen deformation (data not shown). These data suggest that ROCK-dependent phosphorylation is crucial for the correct organization of MLC and force generation. Both recombinant ROCK1 and ROCK1 immune-precipitated from MTLn3E cells could phosphorylate MLC on T18 and S19 in vitro

deformation is shown; we determined this by sampling 50–100 points within 50  $\mu$ m of a cell and averaging 8–10 cells from two or three independent experiments. The asterisk indicates  $p < 0.01$  versus the control (Student's T test).

(F) The effect of 10  $\mu$ M Y27632 or 5  $\mu$ M H1152 on the ability of MTLn3E cells to invade 20  $\mu$ m or more in 24 hr. The average of at least three independent experiments with standard errors is shown; typically 200 cells were analyzed for each experimental condition.

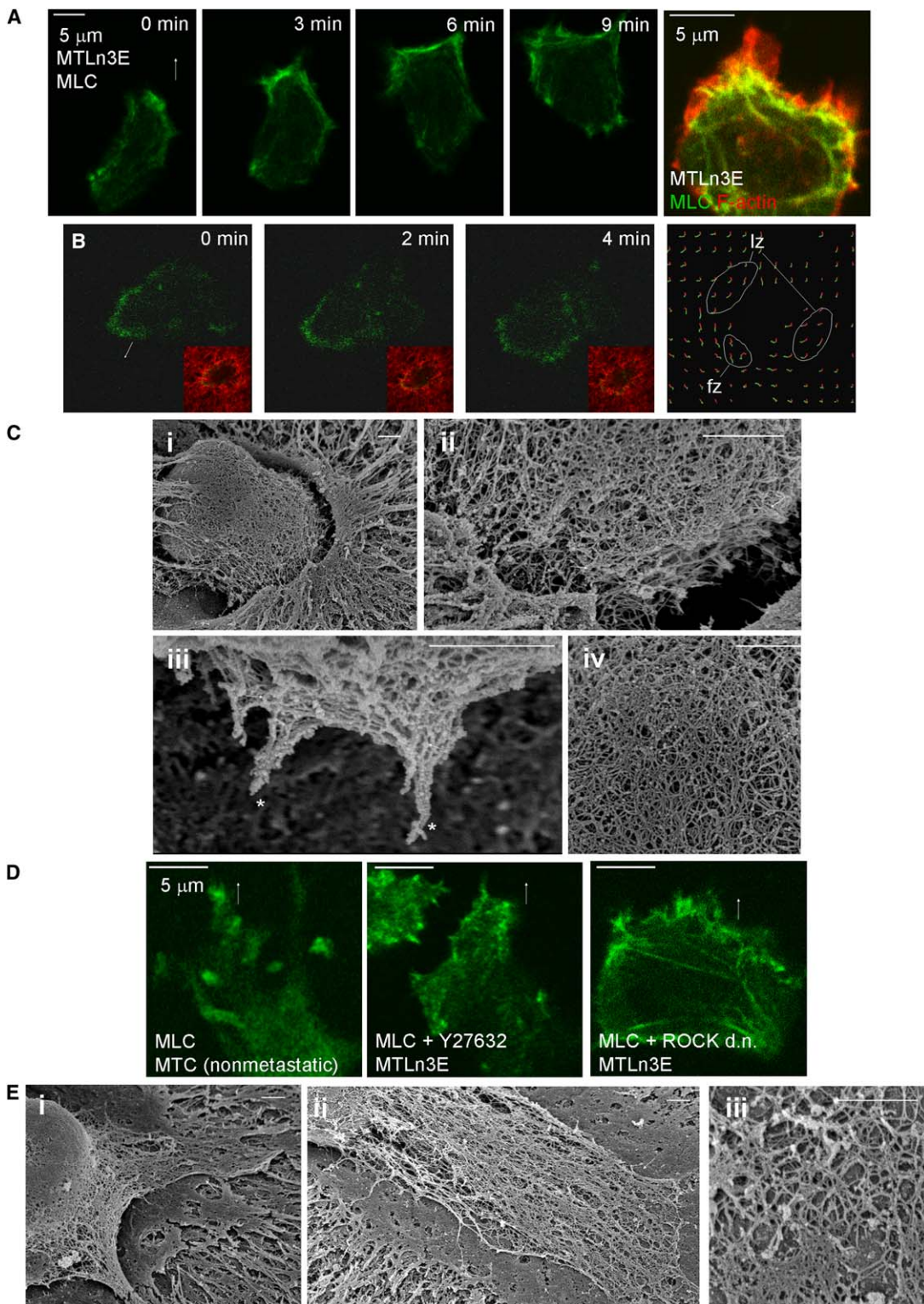


Figure 2. Regulation of Actin and MLC Organization by ROCK in Invading MTLn3E Cells

(A) Images from a time-lapse series of GFP-MLC (green) in an MTLn3E cell moving in a collagen I matrix; the arrow indicates the direction of the movement. Right-hand panel shows MLC organization in a fixed cell costained with phalloidin (red) to reveal F-actin.

(B) Images from a time-lapse series of mRFP-MLC (green) moving a FITC collagen I matrix (red, inset panels). Right-hand panel shows deformation analysis of the cell shown in left-hand panels; fz highlights the area in front of the invading cell, and lz highlights the areas around the side of the invading cell.

(C) SEM images showing F-actin in MTLn3E cells; (i) shows a control cell invading into gel (invading protrusion is labeled with a black arrow), (ii), (iii), and (iv) show actin behind the invading edge, an invading edge, and cortical actin, respectively (white arrowheads indicate densely bundled actin, and asterisks indicate actin-rich protrusions). The scale bar represents 1 micron.

(Figure S4B), suggesting that ROCK may directly phosphorylate MLC in vivo. Next, we tested whether ROCK did indeed regulate MLC phosphorylation in MTLn3E cells. Figure 3C shows that treatment of MTLn3E cells with H1152 to inhibit ROCK reduced the phosphorylation of MLC2 (similar results were obtained with Y27632; data not shown). Inhibition of MLCK alone had only a slight effect on MLC phosphorylation, whereas combined inhibition of ROCK and MLCK almost completely inhibited MLC phosphorylation. These data support the idea that ROCK and MLCK regulate distinct pools of MLC [16, 17]. Immunofluorescence of MTLn3E cells invading into collagen revealed numerous spots of phosphorylated MLC concentrated in the MLC bundle just behind the F-actin-rich protrusion (Figure 3D). Treatment with either H1152 or Y27632 reduced the phosphorylation and organization of MLC near the F-actin-rich protrusion, whereas inhibition of MLCK did not affect MLC phosphorylation or organization in this zone. We obtained similar results by using siRNA against MLCK. Imaging of cells treated with ML-7 showed that these cells retained MLC bundles at the cell cortex but did not efficiently extend protrusions (data not shown). These data demonstrate that ROCK, but not MLCK, regulates the phosphorylation of MLC in a zone just behind the F-actin-rich protrusion; therefore, we investigated whether ROCK protein was localized in this zone. Figure 3E shows that ROCK1 is concentrated within areas of the actin-rich protrusion and just behind the protrusion, but we were unable to convincingly localize ROCK2 or MLCK in this region (Figure 3E; data not shown). Together, these data suggest a novel role for ROCK1 in regulating MLC phosphorylation at the front of the cell immediately subsequent to the formation of the actin-rich protrusion. ROCK can also phosphorylate LIMK; however, activation of LIMK antagonizes the motility of MTLn3 cells because active cofilin is required for the directed movement of MTLn3 cells [18–20]. Therefore, regulation of LIMK is not the crucial positive role of ROCK in cell invasion.

We next asked if overexpression of ROCK1 or activation of ROCK function by expression of constitutively active RhoA could promote the cortical bundles of MLC in cells that normally lack these structures. Overexpression of ROCK1 in nonmetastatic MTC cells promoted the cortical association of MLC but did not have much effect on MLC organization in cell protrusions (Figure 3F). Whereas constitutive activation of ROCK by RhoAV14 caused the formation of MLC bundles all around the cell cortex and antagonized the formation of cell protrusions, this effect was reversed by blockade of ROCK function with Y-27632 (Figure 3F). Together, these data demonstrate that activation of ROCK function is sufficient to concentrate MLC at the cell cortex. We also performed invasion assays to determine if alteration of MLC organization was sufficient to confer invasive behavior on noninvasive MTC cells. Neither overexpression of ROCK1 nor overexpression of RhoAV14 was sufficient to drive the invasion of MTC cells. We speculate that this is because although activation of ROCK

function was able alter the organization of MLC, many other coordinated changes in the actin machinery are needed to drive cell invasion [5].

To investigate the organization of the actomyosin network in vivo, we generated MTLn3 cells that stably expressed MLC-GFP and injected them orthotopically into the mammary fat-pad of mice. Western blot analysis showed that the level of MLC-GFP expression in these cells was similar to the level of endogenous MLC (data not shown). Figure 4 shows that MLC was clearly localized to the cortex of the majority of the cells. Live imaging of the tumors revealed that MLC was recruited to extending cell protrusions and was often organized perpendicularly to the direction in which the protrusion was being extended (Figure 4B and Movie S10). Consistent with our in vitro analysis was our observation of some collagen fibers' localized deformation near dynamic cells at the tumor margins (Movie S10, mid-left area); this observation indicates that significant amounts of force are generated at tumor margins. In contrast, MLC was not cortically organized in nonmetastatic MTC tumors but was more diffuse with some occasional fine bundles and spots of MLC (Figure 4A). No deformation of the collagen matrix was observed in time-lapse movies of MTC tumors (data not shown).

To determine if ROCK regulates MLC in vivo, we injected Y27632 intraperitoneally in tumor-bearing mice and analyzed the phosphorylation and distribution of MLC. Figure 4C shows that Y27632 reduced the phosphorylation of MLC in vivo. Intravital imaging of tumors in Y27632-treated mice revealed that the localization of MLC was dramatically altered; it was no longer organized in bundles around the cortex and behind the invading edge of the cell but was more diffusely localized in the cytoplasm with occasional punctate patches around the cell margin (Figure 4A). Next, we next analyzed time-lapse movies to determine if inhibition of ROCK also affected cell motility. Table 1 shows that Y27632 treatment reduced the number of moving tumor MTLn3E cells by 70%; we obtained similar results by using A431 carcinoma cells that also exhibit amoeboid cell motility in vivo (Table 1; data not shown). There was also a dramatic reduction in the number of rapidly moving non-tumor cells in Y27632-treated animals (these cells are visible as “dark shadows” moving among the fluorescent tumor cells).

MMP function was not required for tumor-cell invasion in vitro (Figure 1C); to test this in vivo, we imaged tumor-bearing mice injected with GM6001. Table 1 shows that injection of GM6001 only marginally reduced the number of moving breast cancer cells and increased the number of moving A431 cells. In contrast, the number of moving host cells was significantly reduced. These results demonstrate that amoeboid tumor cell motility in vivo is ROCK dependent but MMP independent; this may partly account for the poor results of MMP inhibitors in clinical trials [1].

We propose the following model of tumor-cell invasion; initially, an F-actin-rich protrusion is extended;

(D) Organization of MLC in MTC and MTLn3E cells; MTLn3E cells were treated with 10  $\mu$ M Y27632 or cotransfected with an inhibitory ROCK1 construct where indicated (the arrow indicates the direction of protrusion extension).

(E) SEM images showing F-actin in MTLn3E cells; (i) and (ii) show protrusions of Y27632- and H1152-treated cells, respectively (white arrows indicate the protrusion extending over the surface of the matrix). (iii) shows cortical actin of an H1152-treated cell. The scale bar represents 1 micron.

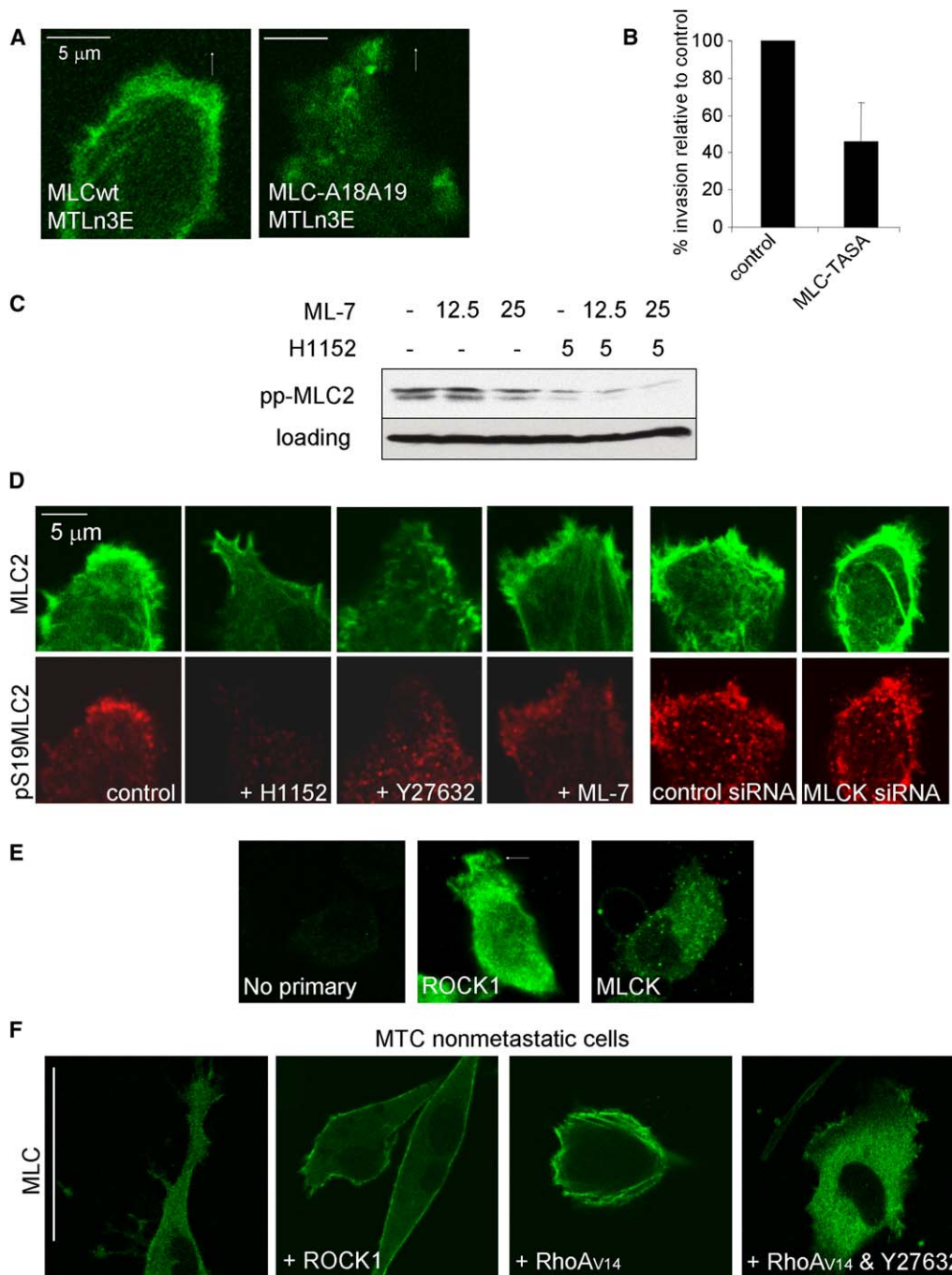


**Figure 3. ROCK Regulates MLC Phosphorylation Behind the Invading Edge**

(A) Representative images from time-lapse series of GFP-MLC or GFP-MLC18A19A in MTLn3E cells in a collagen I matrix; the arrow indicates the direction of the protrusion.

(B) The effect of transfection of MLC-TASA-GFP on the invasion of MTLn3E cells relative to control cells transfected with either GFP or YFP (the average of three experiments is taken; the standard error is shown).

(C) The effect of 12.5  $\mu$ M ML-7, 25  $\mu$ M ML-7, or 5  $\mu$ M H1152 on MLC2 phosphorylation in MTLn3E cells; one representative example of at least three experiments is shown.

(D) Images show MLC2 and phosphoS19-MLC2 localization in untreated, 5  $\mu$ M H1152, 10  $\mu$ M Y27632, or 25  $\mu$ M ML-7-treated MTLn3E cells and control-irrelevant or MLCK siRNA-transfected cells; MLC is shown in red; phospho-MLC2 S19 is shown in green.

(E) Localization of ROCK1 and MLCK in invading MTLn3E cells is shown in green.

(F) Images show MLC2 localization in mock-transfected, ROCK-transfected, RhoAV14-transfected, or RhoAV14-transfected cells treated with 10  $\mu$ M Y27632 in MTC cells. The scale bar represents 50  $\mu$ m.

this is ROCK independent. Subsequently, cell-ECM adhesions form to connect the F-actin network to the ECM; this is also ROCK independent but may be MLCK

dependent [17]. ROCK1 localizes to the invading protrusion, promotes MLC phosphorylation, and enables productive actomyosin interactions leading to the formation

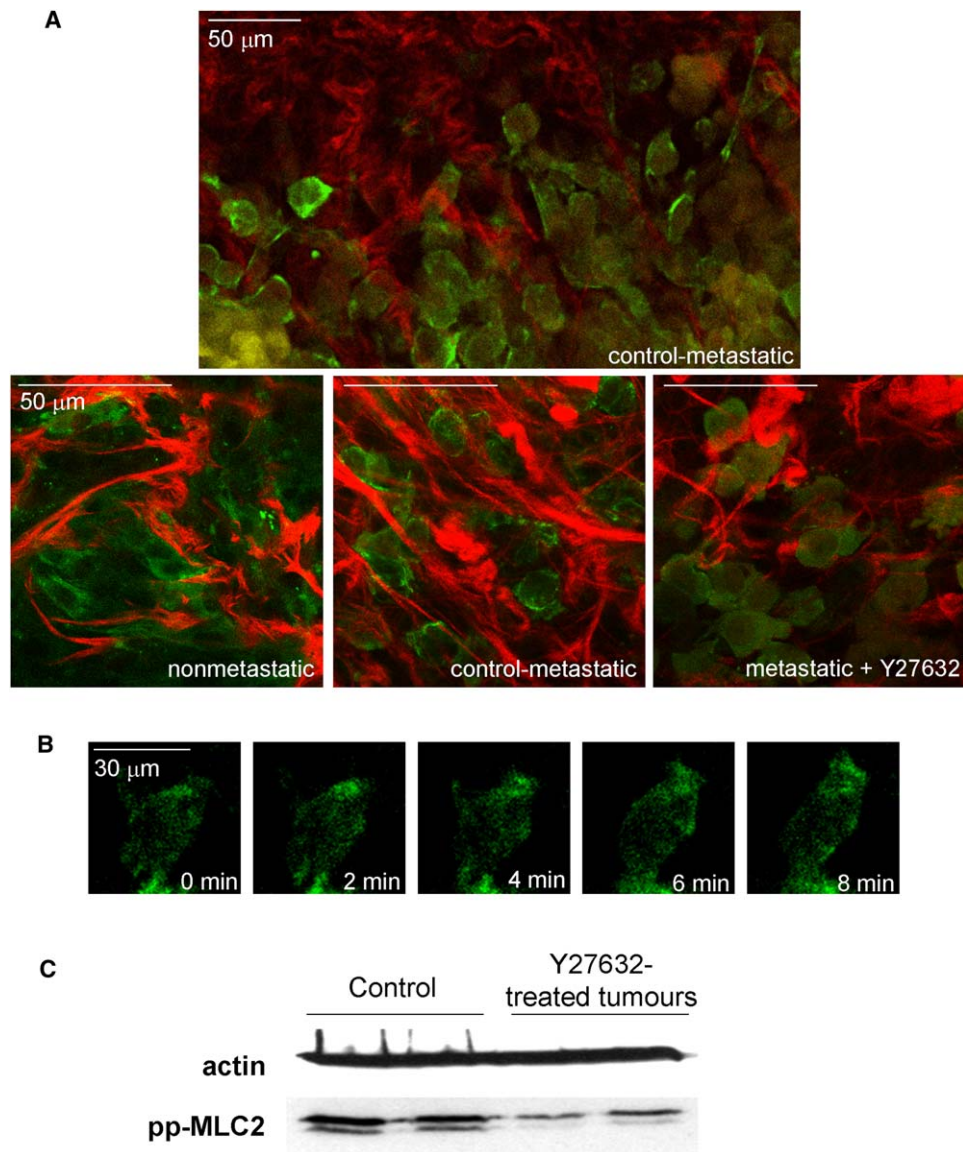


Figure 4. Organization of MLC In Vivo

(A) Metastatic MTLn3 or nonmetastatic MTC cells stably expressing MLC-GFP were injected into the mammary fat-pad of young adult female mice and allowed to form a tumor. After 2–3 weeks, mice were injected with PBS (control) or Y27632; 40–200 min later, living tumors were imaged with a multiphoton laser scanning microscope. MLC-GFP is shown in green; collagen second harmonic signal is shown in red. An asterisk denotes a cell shown in greater detail in (B).

(B) A series of time-lapse images of MLC-GFP localization in the cell marked with an asterisk in (A).

(C) Lysates of MTLn3E tumors from either mice injected with either PBS or Y27632 were Western blotted for phospho-S19 MLC2 or actin (loading control).

of a dense contracting actin mesh behind the invading cell edge. This area may be analogous to the lamella described in some two-dimensional studies [21]. The cell-ECM adhesions are formed predominantly ahead of this zone of actomyosin contractility; therefore, the net effect of the actomyosin contraction is to move the F-actin meshwork of the cell cortex, and hence the whole cell body, toward the adhesions at the front of the cell. As a result of this contraction, actin and MLC are aligned in bundles that are perpendicular to the direction of movement; this is similar to the mechanism proposed by Svitkina and Borisy for fish keratinocyte motility [22]. This region of dense bundled actin is continuous with

the cortical actin, and continued contraction around the cell cortex will cause the cell body to move forward. ROCK also regulates the localization of MLC to the cell cortex and the density of the cortical actin meshwork. Contraction of this network at the sides and rear of the cell will generate hydrostatic pressure that may aid the extension of the protrusion at the front of the cell. In 3D environments, the surrounding ECM will provide resistance to movement of the cell body toward the adhesions at the front of the cell; however, MTLn3E cells can overcome this by generating sufficient force to deform the collagen and couple movement of the invading protrusion to the cell body. If cells are moving in an

**Table 1. Quantification of the Number of Cell-Movement Events in Orthotopic Breast MTLn3 Tumors or Subcutaneous SCC A431 Tumors in Control, GM6001-Treated or Y27632-Treated Animals**

	Control	+GM6001	+Y27632
Number of breast cancer cells moving (events/mm <sup>2</sup> /hr)	102	81	30
Number of nontumor cells moving (events/mm <sup>2</sup> /hr)	101	11	13
Number of SCC cells moving (events/mm <sup>2</sup> /hr)	65	143	22

Tumor cells were identified on the basis of fluorescent-protein expression; nontumor cells in breast MTLn3 tumors were visible as “shadows” moving among labeled tumor cells. Data are taken from imaging four tumors at four different sites in each tumor for each experimental condition; to enable a comparison, we divided the total number of events observed by the area of tumor imaged and the length of time the tumor was imaged.

environment such as on a two-dimensional substrate that does not provide significant resistance to translocation of the cell body, then less force will be required and ROCK activity may be dispensable [23].

The data presented here show that amoeboid tumor cell motility is ROCK dependent but MMP independent. Proteases are not needed because ROCK-dependent regulation of MLC generates sufficient force to deform the ECM and thereby enable cell movement.

#### Experimental Procedures

##### Cell Lines and Plasmids

MTLn3 cells were originally isolated by Welch and Nicolson [24]; MTLn3E cells are described in [7]. GFP-Zyxin was a gift from F. Gertler described in [25]; GFP-MLC and GFP-MLC A18A19 were gifts from M. Olson [15]; details of RhoAV14, ROCK1, and mRFP-MLC are available on request. EF-ROCK1 deltaNIA contains amino acids 945–1355 of human ROCK1 with I1009 mutated to A. Cells were transfected with Fugene-6 in accordance with the manufacturer's instructions. Dharmacon SMARTpool siRNA M-087114-00-0010 was used to target MLCK; cells were transfected with Oligofectamine in accordance with the manufacturer's instructions.

##### Antibodies and Inhibitors

Antibodies used were as follows: phosho-S19 MLC2 (Cell Signaling #3671), phosho-T18S19 MLC2 (Cell Signaling #3674), MLCK (Sigma M7905), ROCK1 (sc-6056 Santa Cruz),  $\beta$ -tubulin (Sigma T 7816), and Zyxin (Synaptic Systems). Inhibitors used were as follows: Aprotinin (Sigma A1153), Blebbistatin (Calbiochem #203391), GM6001 (Calbiochem #364205), H1152 (Calbiochem #555550), Leupeptin (Sigma L 2884), and Y27632 (Tocris #1254).

##### Kinase Assays

Kinase assays were performed essentially as described in [26]. Recombinant ROCK1 was purchased from Upstate (cat #14-601). ROCK1 was immunoprecipitated with goat anti-ROCK1 (sc-6056 Santa Cruz). Recombinant MLC2 was prepared in BL21 *E. coli* (details available on request). Phosphorylation status was analyzed by Western blot with phosho-S19 MLC2.

##### Invasion Assays and Imaging

Collagen I invasion assays were performed as described by Goswami et al. [6] with 4–4.5 mg/ml collagen I (BD Bioscience catalog #354249). For immunofluorescence and time-lapse studies, cells were plated on top of a 4–4.5 mg/ml collagen I gel. For gel deformation analysis, 0.1 mg/ml FITC collagen (Sigma C4361) was added to the collagen I gel. For immunofluorescence studies, cells were fixed in 4% paraformaldehyde and permeabilized with 0.2% Triton X-100 before they were rinsed with phosphate Buffered Saline (PBS) and

blocked with 5% BSA. Primary antibodies were diluted 1:50, and secondary antibodies from Molecular Probes were 1:200, and TRITC-phalloidin (Sigma P1951) was used at 250  $\mu$ g/ml.

##### Gelatin Zymography

HT1080 or MTLn3E cells were cultured for 18 hr in serum-free media supplemented with 2.5% chemically defined lipid concentrate (GIBCO 11905-031) and, where indicated, 5 mM H1152 or 10  $\mu$ M GM6001 + 10  $\mu$ M Aprotinin + 10  $\mu$ g/ml Leupeptin before the media was removed and put through a 0.45  $\mu$ m filter. After the addition of a 20 $\times$  concentration of the protein content with Amicon Ultra 30,000 MWCO spin columns (Millipore), an equal volume of non-reducing SDS-PAGE buffer was added to the cells. Samples were analyzed with 10% acrylamide nonreducing SDS-PAGE containing 1.5 mg/ml gelatin before zymography was carried out as described in [27].

##### Adhesion Assays

Adhesion to collagen I was determined as described in [28] with Chemicon-coated strips (cat. no. ECM104).

##### SEM

Cells were plated on top of Matrigel (BD Bioscience 354234) in the presence or absence of inhibitors; after 16 hr, cells were extracted and fixed according to the method of Bailly et al. [29]. In brief, cells were rinsed twice in Buffer C + 1% BSA + 0.25% Triton X-100 + 5  $\mu$ M phalloidin for 1 min before fixation in cytoskeleton stabilizing solution + 0.5% glutaraldehyde + 0.25% Triton X100 + 5  $\mu$ M phalloidin. Samples were critical-point dried before sputter coating; analysis was performed with a JOEL FESEM 6700 (details available on request).

##### In Vivo Imaging

One million MTLn3 cells stably expressing MLC-GFP were injected under the nipple of 5 to 6-week-old nude mice. A431-GFP cells were injected subcutaneously. After 16–24 days, mice were anaesthetized with isoflurane, and a skin flap was cut to expose the tumor before the mouse was positioned on an LSM510 laser scanning microscope connected to a Chameleon Coherent Ti-Sapphire laser tuned to 850 nm [30]. Anesthesia was maintained while time-lapse movies were made of the tumors. Thirty to forty minutes before imaging, mice were injected intraperitoneally with 100  $\mu$ l PBS, 1 mg of Y27632 dissolved in 100  $\mu$ l PBS, or 0.75 mg of GM6001 dissolved in 100  $\mu$ l PBS + 12.5% DMSO (GM6001 was also injected 16 hr before imaging).

##### Supplemental Data

Supplemental Data include four figures and ten movies and can be found with this article online at <http://www.current-biology.com/cgi/content/full/16/15/1515/DC1/>.

##### Acknowledgments

J.B.W. and J.S.C. are funded by National Institutes of Health grant CA100324; S.E.P., S.G., and E.S. are funded by Cancer Research UK. We thank Chris Marshall and lab members for discussions and comments on the manuscript. We apologize to colleagues whose work we could not cite because of manuscript space constraints.

Received: November 9, 2005

Revised: May 20, 2006

Accepted: May 31, 2006

Published: August 7, 2006

##### References

- Overall, C.M., and Kleinfeld, O. (2006). Tumour microenvironment—opinion: Validating matrix metalloproteinases as drug targets and anti-targets for cancer therapy. *Nat. Rev. Cancer* 6, 227–239.
- Egeblad, M., and Werb, Z. (2002). New functions for the matrix metalloproteinases in cancer progression. *Nat. Rev. Cancer* 2, 161–174.

3. Sahai, E., and Marshall, C.J. (2003). Differing modes of tumour cell invasion have distinct requirements for Rho/ROCK signaling and extracellular proteolysis. *Nat. Cell Biol.* 5, 711–719.
4. Wolf, K., Mazo, I., Leung, H., Engelke, K., von Andrian, U.H., Derjugin, E.I., Strongin, A.Y., Brocker, E.B., and Friedl, P. (2003). Compensation mechanism in tumor cell migration: Mesenchymal-amoeboid transition after blocking of pericellular proteolysis. *J. Cell Biol.* 160, 267–277.
5. Wang, W., Wyckoff, J.B., Frohlich, V.C., Oleynikov, Y., Huttelmaier, S., Zavadil, J., Cermak, L., Bottinger, E.P., Singer, R.H., White, J.G., et al. (2002). Single cell behavior in metastatic primary mammary tumors correlated with gene expression patterns revealed by molecular profiling. *Cancer Res.* 62, 6278–6288.
6. Goswami, S., Sahai, E., Wyckoff, J.B., Cammer, M., Cox, D., Pixley, F.J., Stanley, E.R., Segall, J.E., and Condeelis, J.S. (2005). Macrophages promote the invasion of breast carcinoma cells via a colony-stimulating factor-1/epidermal growth factor paracrine loop. *Cancer Res.* 65, 5278–5283.
7. Xue, C., Wyckoff, J., Liang, F., Sidani, M., Violini, S., Tsai, K.L., Zhang, Z.Y., Sahai, E., Condeelis, J., and Segall, J.E. (2006). Epidermal growth factor receptor overexpression results in increased tumor cell motility in vivo coordinately with enhanced intravasation and metastasis. *Cancer Res.* 66, 192–197.
8. Vanni, S., Lagerholm, B.C., Otey, C., Taylor, D.L., and Lanni, F. (2003). Internet-based image analysis quantifies contractile behavior of individual fibroblasts inside model tissue. *Biophys. J.* 84, 2715–2727.
9. Burton, K., Park, J.H., and Taylor, D.L. (1999). Keratocytes generate traction forces in two phases. *Mol. Biol. Cell* 10, 3745–3769.
10. Oliver, T., Dembo, M., and Jacobson, K. (1999). Separation of propulsive and adhesive traction stresses in locomoting keratocytes. *J. Cell Biol.* 145, 589–604.
11. Meshel, A.S., Wei, Q., Adelstein, R.S., and Sheetz, M.P. (2005). Basic mechanism of three-dimensional collagen fibre transport by fibroblasts. *Nat. Cell Biol.* 7, 157–164.
12. Straight, A.F., Cheung, A., Limouze, J., Chen, I., Westwood, N.J., Sellers, J.R., and Mitchison, T.J. (2003). Dissecting temporal and spatial control of cytokinesis with a myosin II inhibitor. *Science* 299, 1743–1747.
13. Riento, K., and Ridley, A.J. (2003). Rocks: Multifunctional kinases in cell behaviour. *Nat. Rev. Mol. Cell Biol.* 4, 446–456.
14. Fukata, Y., Amano, M., and Kaibuchi, K. (2001). Rho-Rho-kinase pathway in smooth muscle contraction and cytoskeletal reorganization of non-muscle cells. *Trends Pharmacol. Sci.* 22, 32–39.
15. Croft, D.R., Coleman, M.L., Li, S., Robertson, D., Sullivan, T., Stewart, C.L., and Olson, M.F. (2005). Actin-myosin-based contraction is responsible for apoptotic nuclear disintegration. *J. Cell Biol.* 168, 245–255.
16. Russo, J.M., Florian, P., Shen, L., Graham, W.V., Tretiakova, M.S., Gitter, A.H., Mrsny, R.J., and Turner, J.R. (2005). Distinct temporal-spatial roles for rho kinase and myosin light chain kinase in epithelial purse-string wound closure. *Gastroenterology* 128, 987–1001.
17. Totsukawa, G., Wu, Y., Sasaki, Y., Hartshorne, D.J., Yamakita, Y., Yamashiro, S., and Matsumura, F. (2004). Distinct roles of MLCK and ROCK in the regulation of membrane protrusions and focal adhesion dynamics during cell migration of fibroblasts. *J. Cell Biol.* 164, 427–439.
18. Chan, A.Y., Bailly, M., Zebda, N., Segall, J.E., and Condeelis, J.S. (2000). Role of cofilin in epidermal growth factor-stimulated actin polymerization and lamellipod protrusion. *J. Cell Biol.* 148, 531–542.
19. Zebda, N., Bernard, O., Bailly, M., Welti, S., Lawrence, D.S., and Condeelis, J.S. (2000). Phosphorylation of ADF/cofilin abolishes EGF-induced actin nucleation at the leading edge and subsequent lamellipod extension. *J. Cell Biol.* 151, 1119–1128.
20. Ghosh, M., Song, X., Mouneimne, G., Sidani, M., Lawrence, D.S., and Condeelis, J.S. (2004). Cofilin promotes actin polymerization and defines the direction of cell motility. *Science* 304, 743–746.
21. Ponti, A., Machacek, M., Gupton, S.L., Waterman-Storer, C.M., and Danuser, G. (2004). Two distinct actin networks drive the protrusion of migrating cells. *Science* 305, 1782–1786.
22. Svitkina, T.M., Verkhovskiy, A.B., McQuade, K.M., and Borisy, G.G. (1997). Analysis of the actin-myosin II system in fish epidermal keratocytes: Mechanism of cell body translocation. *J. Cell Biol.* 139, 397–415.
23. Hooper, S., Marshall, J.F., and Sahai, E. (2006). Tumour cell migration in 3D. *Methods Enzymol.* 406, 625–643.
24. Welch, D.R., and Nicolson, G.L. (1983). Phenotypic drift and heterogeneity in response of metastatic mammary adenocarcinoma cell clones to adriamycin, 5-fluoro-2'-deoxyuridine and methotrexate treatment in vitro. *Clin. Exp. Metastasis* 1, 317–325.
25. Rottner, K., Krause, M., Gimona, M., Small, J.V., and Wehland, J. (2001). Zyxin is not colocalized with vasodilator-stimulated phosphoprotein (VASP) at lamellipodial tips and exhibits different dynamics to vinculin, paxillin, and VASP in focal adhesions. *Mol. Biol. Cell* 12, 3103–3113.
26. Coleman, M.L., Sahai, E.A., Yeo, M., Bosch, M., Dewar, A., and Olson, M.F. (2001). Membrane blebbing during apoptosis results from caspase-mediated activation of ROCK I. *Nat. Cell Biol.* 3, 339–345.
27. Kamiya, N., Kishimoto, T., Suzuki, H., Sekita, N., Nagai, Y., Oosumi, N., Kito, H., Tochigi, N., Shinbo, M., Nemori, R., et al. (2003). Increased in situ gelatinolytic activity in renal cell tumor tissues correlates with tumor size, grade and vessel invasion. *Int. J. Cancer* 106, 480–485.
28. Vial, E., Sahai, E., and Marshall, C.J. (2003). ERK-MAPK signaling coordinately regulates activity of Rac1 and RhoA for tumor cell motility. *Cancer Cell* 4, 67–79.
29. Bailly, M., Macaluso, F., Cammer, M., Chan, A., Segall, J.E., and Condeelis, J.S. (1999). Relationship between Arp2/3 complex and the barbed ends of actin filaments at the leading edge of carcinoma cells after epidermal growth factor stimulation. *J. Cell Biol.* 145, 331–345.
30. Sahai, E., Wyckoff, J., Philippart, U., Segall, J.E., Gertler, F., and Condeelis, J. (2005). Simultaneous imaging of GFP, CFP and collagen in tumors in vivo using multiphoton microscopy. *BMC Biotechnol.* 5, 14.